Turbulence Phenomena in Drag Reducing Systems

F. A. SEYER and A. B. METZNER

University of Delaware, Newark, Delaware

An analysis based on the Townsend-Bakewell model of the eddies in the wall regions of turbulent shear flows shows that viscoelastic fluid properties must lead to significant reductions in the rate of production of turbulent energy. This analysis in turn leads to the proper form of the similarity laws for drag reducing fluids, heretofore deduced empirically.

Measurements of the axial and radial turbulence intensities for flow through smooth round tubes are reported, as are measurements of the time-averaged velocity profiles and the drag coefficients. These indicate that for solutions exhibiting drag reduction at all Reynolds numbers the flow may be transitional to Reynolds numbers of the order of 10^5. This transitional flow consists of alternating patches of laminar and turbulent fluid, within each of which the flow characteristics are approximately similar to those of Newtonian fluids. At high Reynolds number conditions with the turbulent field fully developed the velocity profile in the core is flatter under drag-reducing conditions than for turbulent Newtonian fluids, a change dependent on the increased isotropy of the turbulent field of the drag-reducing fluid. These effects appear to be a result of increases in the time scales of the radial fluctuations caused by the fluid properties.

Design calculations based upon the present results suggest that in large diameter pipelines, or in boundary layers on large objects, drag reduction may not be attainable under conditions of practical interest until fluids having relaxation times an order of magnitude larger than those presently available, but with comparable viscosity levels, are developed or, alternately, until fluids exhibiting Weissenberg numbers which do not change with deformation rate, can be found.

A growing number of studies have been undertaken which aim to characterize or elucidate the physical aspects of drag reduction. Several of these (*7, 14, 20, 24, 35, 39, 46*) include sufficient ranges of the primary variables such as tube size, the polymeric additive used and its concentration to illustrate the varied nature and extent of drag reduction and the difficulty of obtaining a general and quantitative understanding of the phenomenon. Although in several instances (*10, 22, 24, 28, 39*) drag reduction data have been correlated empirically and several theoretical analysis have been presented (*11, 16, 41, 42*) little consistent information, pertinent to the processes involved in drag reduction, has evolved. Compounding this problem is the utility of measurements using the usual tools of research in turbulence, impact, and hot-wire probes, which has been severely questioned (*2, 15, 23, 25, 36*) and remains in doubt for viscoelastic fluids. Thus the several experimental investigations in which such tools were employed (*2, 12, 13, 28, 44, 46*), though clearly of qualitative interest, possess a quantitative utility which remains to be determined.

THE STRUCTURE OF TURBULENCE IN THE WALL REGION

The comprehensive data of Laufer (*19*) for Newtonian fluids serve to illustrate the importance of the wall region ($y^+ < 30$) in governing the turbulence processes of interest. In particular it is shown that all of the terms appearing in the energy field equations reach sharp maxima here. The deductive arguments of Townsend (*43*) illustrate concisely how the parameters governing the flow in the wall region govern the major macroscopic properties of the flow, such as the pressure drop and the velocity profile. In the near wall region, or equivalently, in the region of constant shearing stress, Townsend shows cylindrical eddies of the same radial scale as the boundary layer thickness govern to a large extent the turbulence processes there. A recent detailed study of the Newtonian flow within this wall region (*3*) has shown that the large eddies exist as counter-rotating pairs with their axes along the mean flow direction. In the lateral direction a diffuse influx of material occurs which is concentrated between the two eddies and rapidly ejected from the boundary layer region owing to the counter-rotation of the eddy pair. The eddy pattern remains defined to the outer edge of the sublayer and as these patterns may be associated with about 50% of the total turbulent energy they must control to a large extent the radial momentum transport rates which exist in the wall region. From the streamline patterns presented by Bakewell a graphical analysis has shown (*38*) that the streamlines are adequately described by:

$$\psi = K(\Delta x)\, y^+ \tag{1}$$

in which K is constant, y^+ represents distance from the wall, and Δx is distance perpendicular to y^+ and the direction of mean flow, measured from the center of the eddy pair.

The kinematics of the flow field represented by Equation (1) are those of elongational or stretching flows. At the center of the eddy structure ($\psi = 0$) the rate of stretching Γ of the fluid element is given simply by:

$$\Gamma = \left(\frac{\partial v}{\partial y}\right)_{\psi=0} = \frac{K u^*}{\nu} \tag{2}$$

which for the assumed structure is independent of distance through the sublayer.

The relevance of Equation (2) arises out of the fact that the stretch rates for viscoelastic materials can be shown to possess effective upper limiting values determined by the physical properties of the material in question, at which the stresses rise to very high levels (*1, 4, 21, 26*). This conclusion does not appear to be severely restricted by choice of any particular empirical constitutive equation but has been suggested as being true for very general constitutive assumptions (*1*).

For purposes of defining the importance of this observa-

F. A. Seyer is at the University of Alberta, Edmonton, Alberta, Canada.

tion in an analysis of turbulence a convected Maxwell model (*47*) will be used to portray the fluid properties. In the Cartesian reference frames of interest this model of the material properties may be written:

$$\tau'_{ij} + \theta \frac{\delta \tau'_{ij}}{\delta t} = 2\mu d_{ij} \tag{3}$$

Equation (3) has been employed in a number of engineering studies (*21, 26, 39, 48*) and, with the exception of its prediction of a zero second normal stress difference is capable of portraying broadly and at least semiquantitatively all the known real effects observed in systems of interest. In particular it has enjoyed some success in depicting the characteristics of Lagrangian-unsteady flows (*21, 26*) similar to those of interest under turbulent conditions. For a fluid described by Equation (3) the deformation rate dependent relaxation time θ may be readily determined from measurements made under conditions of a steady laminar shearing flow, for which:

$$\theta = \frac{\tau_{11} - \tau_{22}}{2\tau_w \gamma} = \frac{N_{ws}}{2\gamma} \tag{4}$$

Applying Equation (3) to steady elongational flows as described by Equation (1) one obtains (*39*):

$$\tau_{yy} = \frac{4\mu\Gamma}{1-(2\theta\Gamma)^2} \tag{5}$$

Equation (5) states that as the term $2\theta\Gamma$ approaches unity the stresses required to sustain such motion must rise to infinity and, in its support, increase in the stress level of two orders of magnitude have been observed experimentally (*4, 21*). Such a result is, however, impossible in a turbulent field in which the stress levels are governed by inertial effects of finite magnitude. Thus, Equation (5) alternately requires that for such finite stress levels:

$$2\theta\Gamma < 1 \tag{6}$$

Comparing the turbulent fields in Newtonian and viscoelastic fluids of the same viscosity level and at a given (high) Reynolds number the stresses (inertial effects) must be comparable in magnitude. If the stretch rate Γ_N in the Newtonian fluid is very large as compared to the term $(1/2\theta)$ for the viscoelastic fluid then the viscoelastic stretch rate will be smaller than Γ_N, so that Equation (6) may be satisfied. Such a decrease corresponds, in the Townsend-Bakewell model of the eddy structure [Equations (1) and (2)] to reduced radial momentum transfer rates or, equivalently, to a reduced drag. It is interesting to note in this connection that Wells and Spangler (*47*) have recently shown experimentally that the sublayer region is of primary importance, though the absence of fluid properties does not enable one to employ their data to confirm the inequality of Equation (6).

SIMILARITY CONSIDERATIONS

The preceding section has demonstrated the importance of elastic properties, described by the relaxation time of the fluid, in controlling the radial momentum transport rates in the wall region. In order to apply these considerations a dimensional analysis is performed parallel to that originally formulated by Millikan (*29*). A similar analysis has been published (*9*) for purely viscous non-Newtonian materials and algebraic details will therefore be omitted in the following.

The overall cross section of the duct is assumed to be divisible into two regions: a turbulent core in which inertial effects are pre-eminent and a wall region in which the constitutive properties of the fluid are also important. One may write that in the wall region:

$$u = f_2(\tau_w, y, \rho, \mu, \theta) \tag{7}$$

and in the turbulent core:

$$U_m - u = f_3(\tau_w, R, y, \rho) \tag{8}$$

So that over the entire section:

$$u = F\ (\tau_w, R, y, \rho, \mu, \theta) \tag{9}$$

The preceding equations are identical to those considered valid for Newtonian fluids except for the addition of the fluid relaxation time as a governing parameter for flow near the wall. Parameters describing the shear dependence of μ and θ need not be included as the viscosity and relaxation time influence the flow only in a region in which the stress is essentially constant. In the following therefore the fluid property parameters are not necessarily assumed to be constants but must be evaluated at the wall shearing stress levels.

Introducing the dimensionless groups:

$$Z = \frac{Ru^*}{\nu}$$

$$\xi = y/R$$

$$\tau = \frac{\theta(u^*)^2}{\nu} \tag{10}$$

Application of the π theorem shows that Equations (7), (8), and (9) may be written in the form:

$$\text{wall region:}\quad \frac{u}{u^*} = f_2(Z\xi, \tau) \tag{7a}$$

$$\text{core region:}\quad \frac{U_m - u}{u^*} = f_3(\xi) \tag{8a}$$

$$\text{centerline:}\quad \frac{U_m}{u^*} = F(Z, \tau) \tag{9a}$$

Assuming that over some region of the tube the velocities and derivatives of velocity with respect to position as given by Equations (7) to (9) coincide, the equations for the region of overlap must be of the form:

$$\frac{U_m - u}{u^*} = -A \ln \xi + C_3 \tag{11}$$

$$\frac{u}{u^*} = A \ln \frac{yu^*}{\nu} + B(\tau) - C_3 \tag{12}$$

The parameters A and C_3 in Equations (11) and (12) may be taken as constants having the Newtonian values since they do not depend upon the dimensionless relaxation time τ. The value of A is commonly taken as 2.46 (*5*). For purely viscous fluids, both Newtonian and non-Newtonian, Equation (11) has been commonly employed over the entire cross section of the turbulent core by allowing C_3 to depend on ξ. Various empirical formulations of $C_3(\xi)$ which have appeared in the literature are concisely summarized by Bogue (*5*) who in turn has developed perhaps the most accurate formulation for $C_3(\xi)$ owing to the extensive data considered. At the tube centerline the correction function is identically zero [Equation (11)] while as noted from Bogue's data, for $0.3 < \xi < 1.0$ the function makes a negligible contribution to the velocity given by Equation (12). For values of the radial position coordinate ξ less than 0.3 the contribution $C_3(\xi)$ generally remains below 10% of the actual velocity. Accordingly it is taken as identically zero, as a first approximation, allowing attention to be focussed on the more important variables.

The function $B(\tau)$ in Equation (12), which describes

the effects of fluid elasticity on the velocity profile, must reduce to the Newtonian value of 5.6 (5) in the limit of a vanishingly small elasticity.

By definition the Fanning friction factor is given by:

$$f = \frac{\tau_w}{\frac{1}{2}\rho V^2} = 2\left(\frac{u^*}{V}\right)^2 \tag{13}$$

in which V denotes the average velocity:

$$V = 2\int_o^1 u\, x\, dx \tag{14}$$

and x is the reduced radial position coordinate r/R.

In order to evaluate the integral appearing in Equation (14) it is usual to assume the validity of Equation (12) over the entire cross section of the tube, for purely viscous fluids. In the case of viscoelastic materials the available velocity profile measurements (*12*) suggest a marked thickening of the sublayer, making it necessary to integrate Equation (14) piece-by-piece (*17*). In the core region Equation (12) will be used; within the sublayer $0 < y^+ < y_l^+$ it will be assumed that the profile is linear as a first approximation, that is $u^+ = y^+$. Setting C_3 equal to zero as discussed earlier Equation (12) gives at $y^+ = y_l^+$:

$$B(\tau) = y_l^+ - A \ln y_l^+ \tag{15}$$

which serves to define y_l^+. It should be noted that although the definition is somewhat arbitrary Equation (15) shows how the thickness of the sublayer must depend on the dimensionless fluid relaxation time τ through dependence on the function $B(\tau)$.

Carrying through the indicated integration and neglecting terms in ξ_l^3 results in:

$$\frac{U_m(1-\xi_l)^2 - V}{u^*} = P\text{-}F(\xi_l) - \xi_l^2 \frac{Ru^*}{\nu} = G\left(\xi_l, \frac{Ru^*}{\nu}\right) \tag{16}$$

wherein, from Newtonian data, $P = 3.60$ and ξ_l is the value of ξ defined by y_l^+. Combining Equations (11), (12), (13), and (16):

$$\sqrt{\frac{2}{f}} = A(1-\xi_l)^2 \ln N_{Re}\sqrt{f} + (1-\xi_l)^2[B(\tau) - A\ln 2\sqrt{2}] - G \tag{17}$$

Equations (12) and (17) constitute the primary results of the dimensional analysis and form the framework for interpreting and finally predicting the behavior of drag reducing systems. In a number of instances (*12, 13, 28*) equations similar to, but less general than, Equation (17), have been presented. For example Elata's (*12*) equation for the drag coefficient may be written:

$$\sqrt{\frac{2}{f}} = A \ln N_{Re}\sqrt{f} - 0.55 + \alpha' \ln \frac{u^{*2}\theta}{\nu} \tag{18}$$

in which the effects of elasticity have been accounted for empirically through a relaxation time θ (assumed constant for a given solution) and the parameter α' which is a function of polymer characteristics and concentration. In Equation (18) the particular form of the intercept function was empirically deduced from the data.

In the limit of vanishingly small elasticity ($\tau \to 0$) Equations (12) and (17) defining the velocity profile and the drag coefficient must reduce to the corresponding equations for Newtonians fluids. At the opposite asymptotic extreme, as τ becomes very large the boundary region must thicken [Equation (15)], and in the limit y_l^+ approaches a limiting value determined by the tube radius. The simplifying assumptions used in Equation (7) and in approximating the wall region with a linear velocity profile cause the analysis to break down, however, as soon as the sublayer thickens sufficiently to encompass an appreciable part of the cross section of the tube and these factors determine the actual limits of applicability of Equations (12), (17), and (18).

EXPERIMENTAL PROCEDURE

Axial and radial components of the instantaneous velocity vector were measured a sufficient number of times to enable calculation of the time-averaged axial velocities as well as the axial and radial intensities, at 5 radial positions in a 1 in. diameter tube. Measurements were made at two values of the Reynolds number in each of two drag reducing systems, as well as in Newtonian fluids to provide a check of the accuracy of the results. The two drag reducing systems studied were chosen to represent the two distinct types of drag reduction observed: (a) highly drag reducing fluids in which drag reduction is observed at all Reynolds numbers in excess of 2,100, and (b) modestly drag reducing fluids in which turbulent Newtonian frictional behavior is observed over some range of (low) Reynolds numbers, followed at higher Reynolds numbers by a region in which drag reduction occurs.

The turbulent velocity data were derived from a series of approximately one hundred photographs of small bubbles entrained in the fluid. Bubbles having on the average a diameter of less than 0.002 in. were introduced by a mixer operating in the fluid storage tank. An estimate of the maximum amount of air in the system (*38*) indicated that the amount of air was much less than 0.0015% by volume. The bubbles were illuminated by passing a 0.040 in. deep horizontal plane of light from a Bausch and Lomb carbon arc lamp through the center of the 1 in. diameter glass tube. The axis of the camera lens was placed perpendicularly to the plane of light; the optical system was calibrated for radial magnification and refraction effects simultaneously by photographing the tip of a 0.0150 in. diameter wire which could be inserted and positioned accurately. Axial magnification was determined directly by photographing a steel rule. With the particular combination of bellows length and camera lens used, the overall magnification of the optical system was about 3.5× with a field of view of about 1.5 in. The light beam was periodically interrupted using a high speed slotted wheel so that each bubble was illuminated for intervals of 1/2400 sec. Measurement of the axial and radial components of the length of the streaks so formed permitted calculation of the axial and radial velocity components. Distances on the photographs were measured to within ± 0.001 in. using a 10-power microscope with a movable micrometer stage. At high Reynolds numbers the number of streaks selected for one velocity measurement was such as to provide an axial length of the order of 1 in. to be measured with the microscope, thus giving

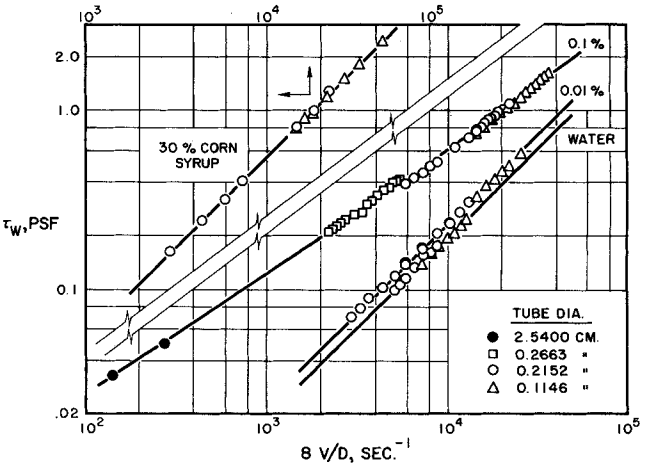

Fig. 1. Experimental measurements of viscous properties of fluids used (water, corn syrup, and 0.01 and 0.1 solutions of ET-597 in water).

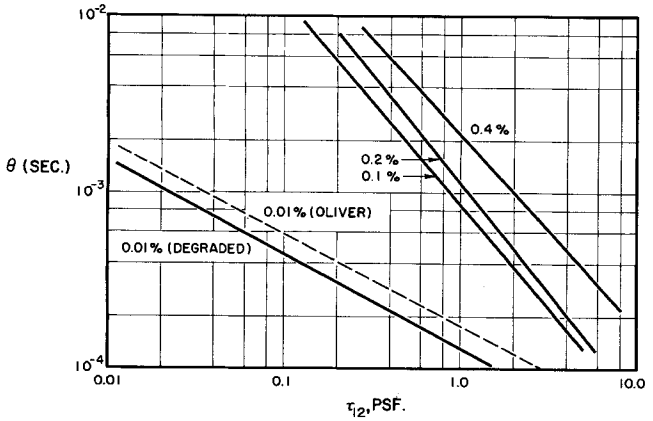

Fig. 2. Relaxation time data, viscoelastic fluids.

negligible errors of measurement. At low Reynolds numbers and for radial velocity measurements an equivalent requirement cannot be applied, owing to the small values of these velocities, and these latter measurements will accordingly be seen to be subject to some error.

Ideally instantaneous velocity measurements are required to determine the root mean square values of the velocity fluctuations, but in fact only the large scale energy-containing eddies contribute significantly to the result. At the higher Reynolds numbers in the present work the fluctuations on a time scale of less than 1/1200 sec. could not be determined. However, recent data (*31*) indicate the time scale characteristic of the dissipative portion of the turbulent spectrum to be about 1/1800 sec. Since the time scales of the energy containing eddies are an order of magnitude larger, the measurements made provide root mean square velocities which appear to contain contributions from all significant frequencies. A detailed consideration of errors associated with analysis of the photographs as well as the statistical limitations of the data is available (*38*).

The fluids used were 0.01% and 0.1% by weight aqueous solutions of ET-597, a high molecular weight polyacrylamide manufactured by Dow Chemical Co. The viscous properties of these viscoelastic fluids, as well as those of the Newtonian fluids used, are presented in Figure 1. These were determined using a capillary tube viscometer described in detail elsewhere (*40*). The elastic properties [the parameter θ in Equation (3)] were estimated using normal stress measurements on equivalent materials (*30, 39*). In order to take into account the fluid degradation in the circulatory system used it was assumed that both the normal and shearing stresses were effected identically [Equation (4)]. Thus in Figure 2 the dashed line represents relaxation times calculated directly from Oliver's data while the solid line represents the estimate for the degraded solution used in this work.

RESULTS

Frictional data are presented in Figure 3. Pressure drop measurements for the 0.01% solution were obtained before and after the photographic runs, which in Figure 3 correspond to the lower and higher values of the friction factors respectively. On the completion of the photographic runs the solution was evidently stable to further degradation, as these photographic data points deviate but slightly from the data obtained later. This is not true in the case of the data for the 0.1% solution.

The data in Figure 3 serve to illustrate clearly the qualitative differences between the solutions which exhibit a large drag reduction and those which display this phenomenen only modestly. The data for the 0.1% solution show that drag reduction occurs at all generalized Reynolds numbers in excess of 2,100. At a generalized Reynolds number of 31,500, corresponding to the conditions of the photographic run, the actual pressure loss is approximately 27% of that for water at the same velocity. In contrast, the 0.01% data show that drag reduction is delayed until a critical Reynolds number is reached, beyond which a modest amount of drag reduction occurs. At a Reynolds number of 144,000 for example, the pressure loss is roughly 55% of the pressure loss for water at the same velocity.

Data defining the experimental conditions at which velocity and intensity measurements were made are presented in Table 1. The analysis of the Townsend-Bakewell eddy pattern considered in Equations (1) to (6), applied to the present data, is summarized in Table 2. To carry out this evaluation the scaling constant K in Equation (2) was determined by equating the radial velocity components of the Townsend-Bakewell eddies to the measured root mean square values of the radial velocities.

Table 1. Experimental Conditions for Turbulence Measurements

Fluid	$\nu w \times 10^5$ sq. ft./ sec.	N'_{Re}	V ft./sec.	u^* ft./sec.
0.1% ET597, run I	4.60	13,370	10.0	0.304
0.1% ET597, run II	3.27	31,500	19.2	0.465
0.01%ET597, run III	1.16	13,500	1.87	0.110
0.01% ET597, run IV	1.16	144,000	20.0	0.678
30% corn syrup	2.56	12,100	3.78	0.235
water	0.964	160,000	18.5	0.824

In view of Equations (2), (5), and (6) one would expect no drag reduction to occur when $2\theta\Gamma_N << 1$, since under these conditions the Newtonian stretch rate Γ_N may be accommodated in viscoelastic fluids with no significant increases in the stresses to levels above those of the Newtonian case. Conversely, as $2\theta\Gamma_N$ approaches values of the order of unity appreciable decreases in the turbulent momentum transport rates should be found. Table 2 shows these trends to be followed, thus supporting not only the qualitative plausibility of this model but suggesting the basis for the quantitative similarity analysis, Equations (7) to (9), to be sound.

Table 2. Relationship between Drag Reduction and Stretch Rates

	$\theta \times 10^4$ sec.	$2\theta\Gamma_N$	$(u^*)_{DR}/(u^*)_N$
run III	9.5	0.06	1.0
run IV	1.4	0.50	0.74
run I	62	2.2	0.53
run II	23	3.4	0.47

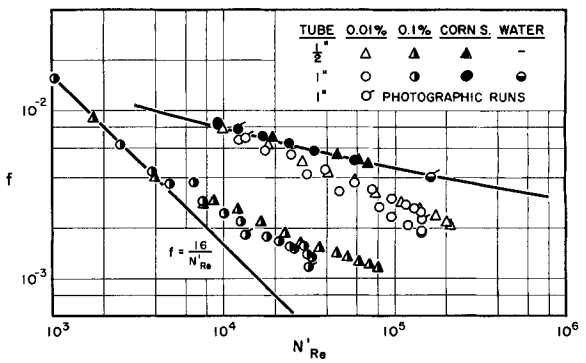

Fig. 3. Drag coefficient results.

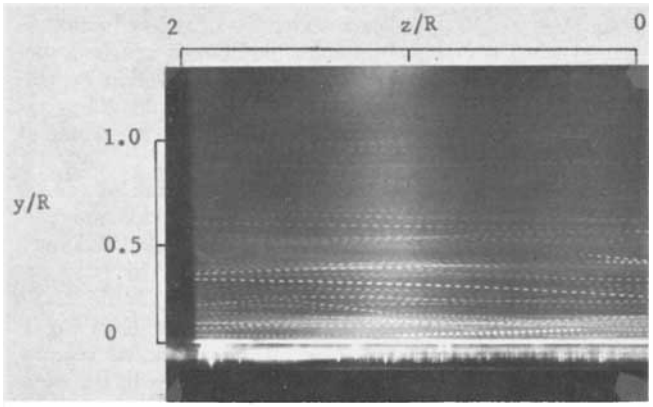

Fig. 4. Streak photographs (a) nondrag reducing conditions. Run III: N_{Re} = 13,500, V = 1.87 ft./sec.

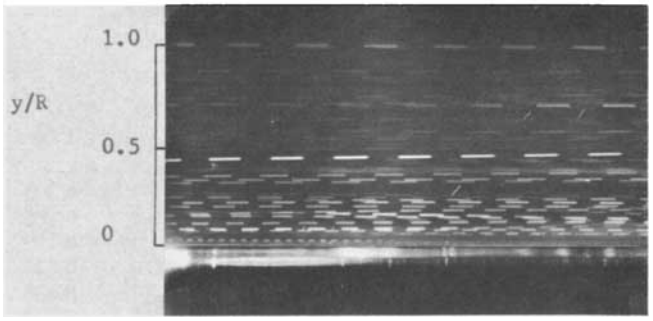

Fig. 4 (b) Drag reducing conditions: Run I: N_{Re} = 13,400, V = 10.0 ft./sec.

Sample streak photographs, representative of the conditions in Table 1, are presented in Figure 4. The time scale corresponding to the length of one streak is, as noted earlier, about 1/2400 sec. The upper of the two photographs displays the characteristics of Newtonian turbulence noted in nondrag reducing systems: large radial velocity fluctuations and a thin wall region, the latter implying low velocity gradients and hence equal streak lengths over the major portion of the velocity field. Conversely Figure (4*b*) reveals a boundary layer extending over most of the tube and a virtual absence of velocity fluctuations. Study of a large number of photographs taken under drag reducing conditions indicate, however, that in both runs I and II (severely drag reducing, see Table 2) infrequent but large radial velocity fluctuations do occur: the flow has an intermittent character with long periods of essentially laminar flow interspersed with bursts of turbulence. The Reynolds numbers, it will be remembered, are 13,370 and 31,500, unusually high for incompletely turbulent fields.

The profiles of the time-averaged or mean velocities are plotted in Figure 5. Excellent agreement was generally obtained between the average bulk velocity determined from the calibrated mass flowmeter and the velocity determined by integration of the velocity profile. The largest discrepancy occurs for run I, in which the difference is 3% of the flowmeter value; for all other runs the discrepancy amounted to less than 1.6%. The 95% confidence limits for the data points were always found to be within ±5% of the point shown (38). The solid lines of Figure 5 represent profiles calculated either from the usual laminar profile equation or from Bogue's (5) logarithmic equation for turbulent conditions. The turbulent data for water and for run III (not drag reducing, see Table 1) are in excellent agreement with the expected turbulent Newtonian profiles.

Under the drag reducing conditions of the 0.01% solution the data, (run IV) show a surprising flat profile in the turbulent core. A similar result, based on hot film measurements in dilute polyethylene oxide solutions, has been noted by Virk (44). Introducing an eddy viscosity one may write:

$$\tau_w (1-\xi) = \mu_e \frac{du}{dr} \tag{19}$$

On consideration of the mechanisms involved in the generation of the turbulent shear stress Phillips (32) has shown the eddy viscosity must be of the form:

$$\mu_e = \hat{A}\,\rho (v')^2 \hat{\theta} \tag{20}$$

in which $\hat{A}$ is a constant and $\hat{\theta}$ represents, on the average, the time scale over which the radial fluctuations remain coherent. Thus, for a given level of shear stress the velocity gradient is governed by the radial intensity and the time scale $\hat{\theta}$. In view of the fact that sudden deformations of viscoelastic fluids lead to very high stress levels (27), as do elongational flows as noted earlier, one would expect $\hat{\theta}$ to be appreciably larger in these systems than in Newtonian fluids, leading to higher eddy viscosities and lower velocity gradients unless the radial intensity term v' is much smaller. In fact, this will be seen to be about the same as in Newtonians, hence the flatter velocity profiles and higher eddy diffusivities are reasonable qualitatively.

The radial and axial turbulence intensity data for the 0.01% solution and the Newtonian fluids used have been plotted in Figure 6. In general the confidence limits for the intensity measurements are much broader than those for the mean velocities, being ±15 to 20% of the plotted values (38).

In Figure 6 the solid lines represent data obtained by Sandborn (34) on air in a 4 in. pipe. The data obtained by Wells, et al. (45) for water in a 0.76 in. tube are

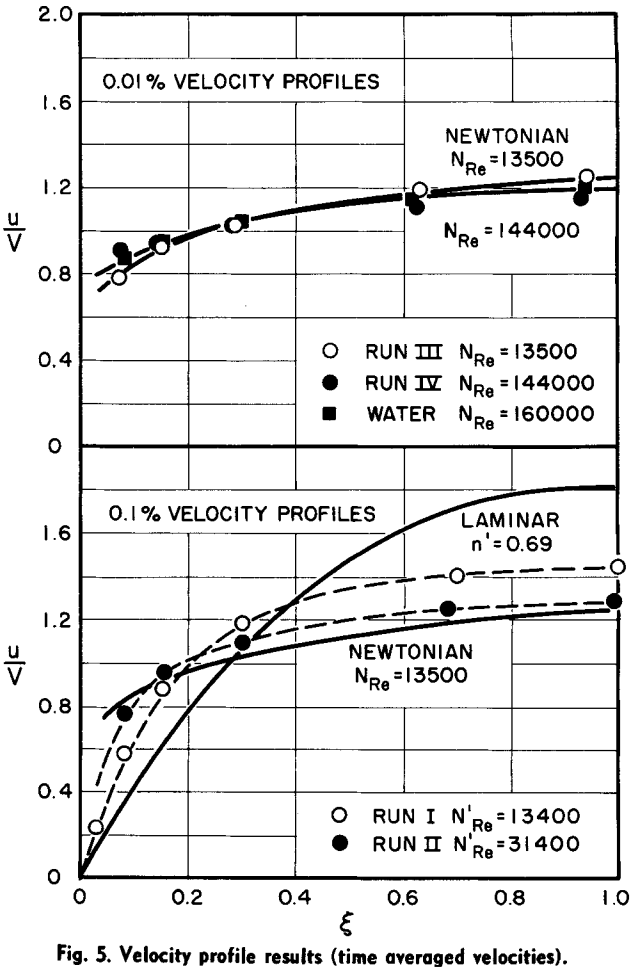

Fig. 5. Velocity profile results (time averaged velocities).

represented by the broken line. Sandborn's measurements are in close agreement with those of Laufer (*19*) and with the measurements in liquid systems by Patterson and Zakin (*31*) and Wells.

Considering the high Reynolds number Newtonian data it is evident that both the axial and radial results are in close agreement with accepted Newtonian data at similar Reynolds numbers. At low Reynolds numbers the present Newtonian data, while consistent with the Reynolds number trends, are generally higher than might be expected. No literature data on radial intensities at $N_{Re} = 12{,}000$ are available for comparison, but in the case of the axial intensities at low Reynolds number the data are approximately 15% higher than Wells' data for water. This difference may be acounted for by random errors in the streak length measurements, as noted earlier. However, for purposes of comparing the Newtonian and viscoelastic data at a given Reynolds number the error is not significant, however as it would be of a comparable magnitude in both cases.

The data for Figure 6 show that when no drag reduction occurs in the viscoelastic fluid (run III) the turbulence intensities of the polymer solution are in close agreement with those of the Newtonian fluid at the same Reynolds number. At the higher Reynolds number (run IV), with the turbulent drag coefficient about 55% that of water it is apparent that all of the points for the axial intensity are roughly 20% lower than the corresponding points for water, while the radial intensity data show close agreement with the water data. Statistically the differences between the corresponding axial intensity data points at $\xi \approx 0.15$, are just significant at the 90% level of confidence. Assuming that the observed lowering of the axial intensity (relative to the radial intensity) is real, a shift toward isotropy has occurred. A lowering of the turbulent Reynolds stress is implied since for isotropic turbulence the Reynolds stress must be zero. This is of course consistent with the experimentally observed lowering of the shearing stress or the drag coefficient.

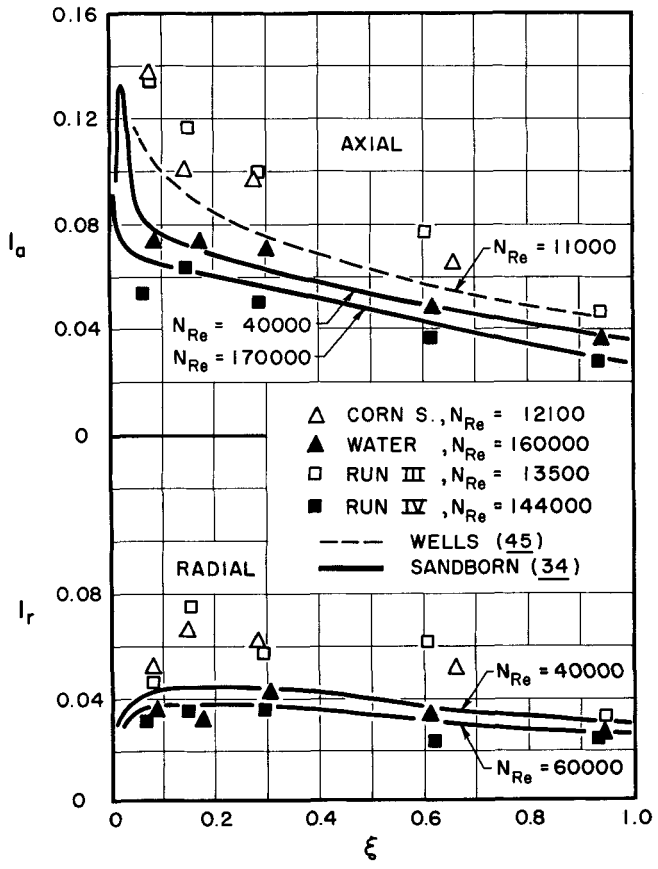

Fig. 6. Turbulence intensities, 0.01% polymeric solution.

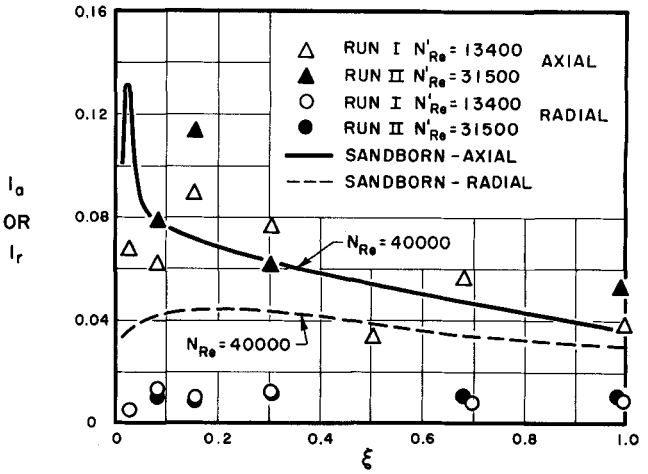

Fig. 7. Turbulence intensities, 0.1% solution.

At the Reynolds numbers considered in this work the 0.1% velocity profiles show large deviations from turbulent Newtonian profiles at the same Reynolds numbers. In Figure 5 the profiles of runs I and II are compared with a turbulent Newtonian profile and with the profile which would exist if the flow were laminar at the same flow rate. Qualitatively the profiles imply that the flow is transitional in that the profiles are neither laminar nor turbulent but between the two. Turbulence data for Newtonian fluids in transitional flow have been reported by Rotta (*33*) and subsequently in summary by Schlichting (*37*). Rotta's measurements show that the flow field in the transitional region consists of alternating patches of laminar and turbulent fluid so that the time-averaged profile must lie between the two profiles.

The suggestion that the flow of 0.1% solutions used in the present work is transitional is supported by two other facts. First, Rotta's measurements indicate that for transitional flow extremely large entrance lengths are necessary for conditions of constant intermittency, or equivalently constant pressure drop, to develop. Even in the case of Reynolds numbers near 2,600 for which the intermittency factor approaches unity in Newtonian systems entry lengths of 300 to 400 diam. are required for the flow to become steady. Although the very large entry lengths of drag reducing systems have been previously noted experimentally (*9*) they seem to have been ignored or unnoticed in a large part of the studies to date. Secondly, the intensity data provide a measure of the intermittent character of the flow. The alternating patches of laminar and turbulent fluid will tend to give rise to very large axial velocity fluctuations, as the velocity at a given radial position fluctuates between the levels associated with laminar and turbulent fields. Unless the intermittency is very low, therefore, one would not expect gross decreases in the axial turbulence intensity from the levels associated with fully developed turbulence. By contrast the radial intensities are highly sensitive to the intermittency of the flow. For example if it is assumed that the intermittency is ½ then out of n measurements $n/2$ will contain no radial fluctuations and the mean square radial velocity will be just ½ of the mean square radial velocity for fully developed turbulence.

Figures 7, in light of the above arguments, shows the flow to be transitional in the highly drag-reducing fluid at both Reynolds numbers studied, 13,400 and 31,500. Further, although the intermittency level of the turbulence has been increased in moving from the lower to the higher Reynolds number the usual sharp transitions in the drag coefficients noted earlier (*39*) have not yet ap-

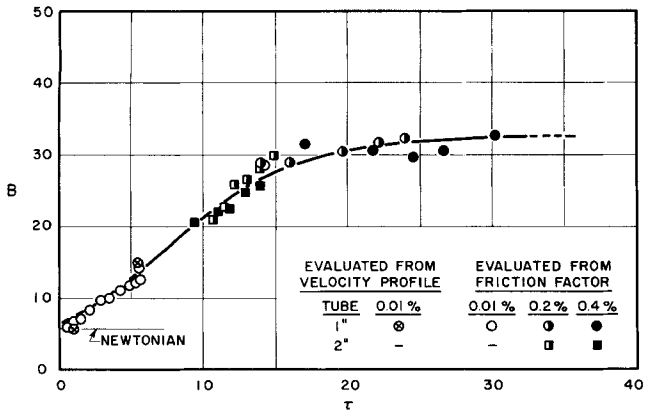

Fig. 8. Experimental evaluation of $B(\tau)$, Equations (12) and (17).

peared in the 0.1% solution data shown in Figure 3, indicating that in small tubes the transition to a full-non-intermittent turbulent field may be delayed to Reynolds numbers of the order of 10^5. Recently available direct measurements of intermittency (*6*), utilizing a pressure-sensitive probe, support the suggestion of a delayed transition to full developed turbulence, even at (polyethylene oxide) solution concentration levels of only 2.5 ppm. Clearly stability studies of the laminar viscoelastic field are of interest.

CONSIDERATION OF SIMILARITY LAWS FOR VELOCITY PROFILES AND DRAG COEFFICIENTS

Equations (12) and (17) yield the turbulent velocity profiles and drag coefficients in terms of three functions which must be determined experimentally: $B(\tau)$, G and ξ_l, the latter two being related through Equation (15). The details of the analysis of the data to obtain these functions (*38*) may be summarized as follows:

The parameter G makes its largest contribution to the data for Newtonian fluids at low Reynolds numbers and use of a constant value, independent of the variables given by Equation (16), appears to suffice. The validity of the value chosen, 3.00, is illustrated in Table 3 in which values of the centerline velocity computed using this value of G are compared with the experimental values obtained for all of the present data, both Newtonian and non-Newtonian. It is seen that the comparison is a good one.

Table 3. Experimental and Calculated Centerline Velocities

Run	U_M (ft./sec.) Calculated	U_M (ft./sec.) Experimental
I	15.3	14.4
II	25.1	24.6
III	2.33	2.34
IV	22.5	23.1
corn syrup	4.76	4.98
water	20.9	22.2

In order to determine $B(\tau)$ over a wide range of values of the dimensionless time ratio τ earlier data (*39*) as well as those of the present investigation were utilized. The resulting experimental function is shown in Figure 8, as determined using all data at Reynolds numbers beyond the transition to fully developed turbulence, the latter assumed to be revealed by discontinuous changes in the drag coefficient-Reynolds number plots. The unavailability of data in small tubes for fluids which were sufficiently dilute to exhibit well-developed turbulence and for which relaxation time measurements were also available, as well as the absence of data for very large ducts, restricts the range of tube diameters studied severely. Nevertheless the essentially linear dependence of $B(\tau)$ upon τ for values of τ less than 15, and the asymptotic constancy of $B(\tau)$ at high values of τ are both results of design importance. A comparison between the experimental drag coefficients with those predicted using Equation (17) and the smooth curve of Figure 7 is shown in Figure 9; the mean absolute deviation between the two is 4.2%.

APPLICATIONS TO DESIGN AND SUMMARY COMMENTS

At high Reynolds numbers those systems which are strongly drag reducing frequently exhibit friction factor-Reynolds number relationships which parallel those of Newtonian fluids. This effect is predicted to occur by Figure 8 whenever $B(\tau)$ is essentially independent of τ, and it thus also predicts the existence of an upper limit to the obtainable drag reduction under turbulent conditions. The drag coefficients for such a maximal drag-reducing fluid may be shown to be analogous to those of a Newtonian fluid exhibiting a transitional Reynolds number of 14,400 (*38*). Still lower drag coefficients could, of course, be obtained if the stability of the laminar field was such as to enable the transition to complete turbulence to be delayed to even higher Reynolds number levels, the above considerations being relevant only when the fluid has finally become fully turbulent. It should be noted that Virk (*44*) has postulated a maximum drag reduction asymptote on the basis of experimental data for several fluids.

In the absence of relaxation time data for the fluid in question it is not possible to predict the frictional behavior *a priori*. Practically, however, this problem may be circumvented without recourse to measurement of the elastic properties of the material, providing it is possible to measure the drag coefficients under turbulent conditions at two flow rates. Using $B(\tau)$ as presented in Figure 8, two measurements of the drag coefficient can be used to estimate two values of the group τ; as it in turn can frequently be represented as a power law function of the wall shearing stress τ_w, with an exponent in the range 0.2 to 0.5 for dilute solutions (*38*), a logarithmic plot of these variables may suffice as an approximate determination of the relevant viscoelastic properties. In

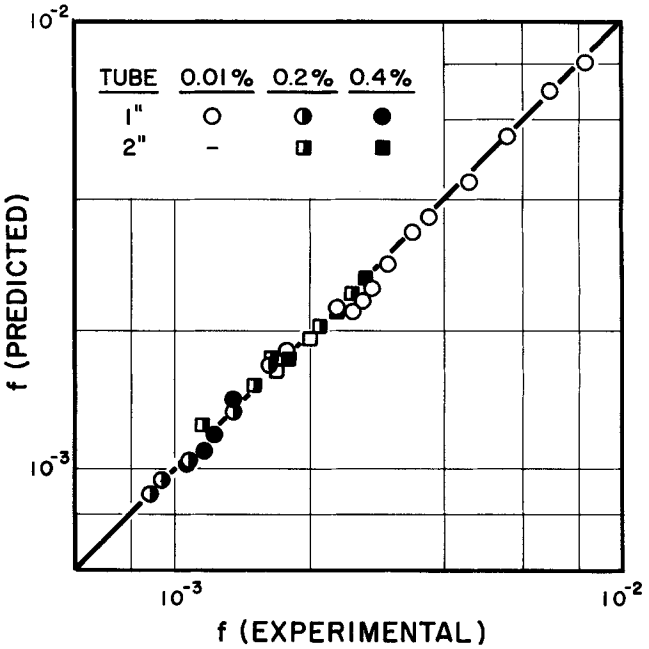

Fig. 9. Comparison of predicted drag coefficients with experimental values.

principle it is also necessary to know the sublayer thickness ξ_l which, however, may be assumed to be zero as a first approximation in determining $B(\tau)$. Using the approximate $B(\tau)$ an adequate estimate of ξ_l follows from Equation (15) which may then be used iteratively to recalculate $B(\tau)$ at the conditions of interest.

The important and commonly observed decrease in drag reduction with increases in tube diameter, at a given Reynolds number, is contained implicitly in Equation (17) through the dependence of $B(\tau)$ (and τ) upon the wall shearing stress. For the dilute (0.01%) solution of the present study it was noted that a Reynolds number of 1.4×10^5 the drag was reduced to 55% of the Newtonian value. Calculations based on Equation (17) and Figures 2 and 8 show that this fluid would be predicted to exhibit no drag reduction at all in a 12 in. diameter duct until Reynolds numbers of nearly 10^6 were reached and would reach a magnitude of 35% at $N_{Re} = 1.8 \times 10^6$. Similarly to achieve a reduction in drag of 55% at $N_{Re} = 1.4 \times 10^5$ a fluid having the viscoelastic properties of the 0.2% solution (Figure 2), but having the same viscosity as the 0.01% solution, would be required. This would appear to necessitate the development of additives which are an order of magnitude superior to those studied to date. A few unpublished data obtained using a 5 in. pipe serve to support both this and the validity of the correlation for such larger ducts. Two routes appear to be available for development of such superior fluids:

1. Systems exhibiting much larger relaxation times, θ, but low viscosity coefficients, could be sought. In view of degradation problems involving very large polymeric molecules the Savins (35) alternative of use of systems forming temporary or reversible viscoelastic structures is of interest.

2. If the Weissenberg number of Equation (4) is independent of deformation rate, then the dependence of the drag reduction upon tube diameter may be shown to disappear except for higher order effects arising out of the ξ_l. This point illustrates the importance of fluid physical property measurements on a wide variety of fluids, to determine which molecular or microrheological structures are likely to lead to such constant (and large!) Weissenberg numbers.

Significantly, it has been noted in studies of Taylor instabilities in Couette flows (*8*, *18*) that the second normal stress difference has a marked effect on the stability of the velocity field. This factor, ignored in all available studies of turbulent drag reducing systems, including the present, could play a substantial role. Thus, though Equations (12) and (17) and Figure 8 present a set of internally consistent design criteria the possibly significant importance of additional rheological properties cannot be overlooked. Their relevance could be such as to cause two fluids having identical relaxation time and viscosity functions to exhibit differences in their drag-reducing characteristics especially under conditions of low to modest Reynolds numbers, in which region the mechanics of the fluid motion may be peculiarly sensitive to transitional or instability phenomena.

ACKNOWLEDGMENT

This work has been supported by the Office of Naval Research, U. S. Navy. Dow Chemical Company supplied the polymeric additive used.

NOTATION

$\hat{A}$ = constant, Equation (20)

A = slope of logarithmic velocity profile, A (Newtonian) = 2.46

B, C_3 = intercept functions for logarithmic velocity profile, $B(0)$ [the Newtonian fluid value] = 5.6

d_{ij} = components of deformation rate tensor

D = tube diameter

f = Fanning friction factor, Equation (13)

f_2, f_3, F = arbitrary functions

G = function; Equation (16). Approximated by a constant value for design purposes: $G \approx 3.00$.

I_a, I_r = relative axial and radial intensities, $I_a = u'/U_m$; $I_r = v'/U_m$

K = scaling constant for large eddy structure

L = length along tube

n = number of instantaneous observations

n' = power law exponent (9)

N'_{Re}, N_{Re} = generalized Reynolds number (9) and Reynolds number based on apparent viscosity at the wall respectively

N_{Ws} = Weissenberg number, ratio of elastic viscous stresses

P = constant of integration = 3.60 for Newtonian fluids, Equation (16)

r = radial position

R = radius of tube

u = local time—averaged axial velocity

u^* = friction velocity $\sqrt{\tau_w/\rho}$

u^+ = dimensionless local velocity = u/u^*

u', v' = axial and radial turbulent intensities

U_m = time-averaged fluid velocity at centerline of duct

v = radial velocity component of eddy

V = bulk (average) velocity

Δx = distance across the large eddies

y = distance from tube wall

y^+ = dimensionless distance from tube wall

y_l^+ = y^+ defined by intersection of linear and logarithmic velocity profiles

Z = Reynolds number based on friction velocity, Equation (10)

Greek Letters

α' = empirical constant, Equation (18)

γ = shear rate

Γ = rate of stretching; Γ_N denotes this term for a Newtonian fluid

θ = fluid relaxation time function

$\hat{\theta}$ = integral time scale as defined by Phillips (32)

μ_e = eddy viscosity

μ = viscosity function; μ_w denotes the viscosity evaluated at the wall shearing stress, τ_w

ν_w = apparent kinematic viscosity evaluated at τ_w

ξ = dimensionless distance from wall = y/R

ξ_l = value of ξ defined by y_l^+

ρ = density

τ = dimensionless time ratio, Equation (10)

τ'_{ij} = components of deviatoric stress tensor

τ_{ij} = components of total stress tensor

τ_w = shear stress at tube wall

ψ = stream function

$\delta/\delta t$ = convected time derivative (48)

LITERATURE CITED

1. Astarita, G., *Ind. Eng. Chem. Fundamentals*, **6**, 257 (1967).
2. ——, and L. Nicodemo, *AIChE J.*, **12**, 478 (1966).
3. Bakewell, H. P., Ph.D. thesis, Pennsylvania State Univ., University Park (1966).
4. Ballman, R. L., *Rheol. Acta*, **4**, 137 (1965).
5. Bogue, D. C., and A. B. Metzner, *Ind. Eng. Chem. Fundamentals*, **2**, 143 (1963).

6. Castro, W. E., Digest of Ph.D. thesis, Univ. West Virginia, Morgantown (1966).
7. Crawford, H. R., and G. T. Pruitt, Rept no. DTMB-1, prepared for David Taylor Model Basin Hydromechanical Lab., Washington, D. C. (1965).
8. Denn, M. M., and J. J. Roisman, *AIChE J.*, **15**, 000 (1969).
9. Dodge, D. W., and A. B. Metzner, *ibid.*, **5**, 189 (1959).
10. Elata, C., and J. Tirosh, *Israel J. Tech.*, **3**, 1 (1965).
11. ———, and M. Poreh, *Rheol. Acta*, **5**, 148 (1966).
12. ———, J. Lehrer and A. Kahanovitz, *Israel J. Tech.*, **4**, 87 (1966).
13. Ernst, W. D., *AIChE J.*, **12**, 581 (1966); *Am. Inst. Aeron. Astronaut. J.*, **5**, 906 (1967).
14. Fabula, A. G., *Proc. 4th Intem. Congr. Rheol.*, 3, 455 (1965).
15. ——— "Proc 6th Naval Hydrodynamics Symposium, Office Naval Res., Washington, D.C.; Ph.D. Thesis Pennsylvania State Univ., University Park (1966).
16. Gadd, G. E., *Nature*, **206**, 463 (1965).
17. Granville, P. S., *Hydromechanics Lab. t. n. no. 61*, David Taylor Model Basin, Washington, D. C. (1966).
18. Giesekus, H., *Rheol. Acta*, **5**, 239 (1966).
19. Laufer, J., *Natl. Advisory Comm. Aeron.* Rept. 1174 (1954).
20. Lummus, J. L., J. E. Fox and D. B. Anderson, *Oil Gas J.* No. 12, 87 (1961).
21. Marshall, R. J., and A. B. Metzner, *Ind. Eng. Chem. Fundamentals* **6**, 393 (1967).
22. Meter, D. M., and R. B. Bird, *AIChE J.*, **10**, 881 (1964).
23. Metzner, A. B., and G. Astarita, *ibid.*, **13**, 550 (1967).
24. ———, and M. G. Park, *J. Fluid Mech.*, **20**, 291 (1964).
25. ———, and F. A. Seyer, "Proc. 6th Naval Hydrodynamics Symposium," Office Naval Res., Washington, D. C. (1966).
26. ———, E. A., Uebler, and C. F. Chan Man Fong, *AIChE J.*, to be published.
27. Metzner, A. B., J. L. White, and M. M. Denn, *ibid.*, **12**, 863 (1966); *Chem. Eng. Prog.*, **62**, 12, 81 (1966).
28. Meyer, W. A., *AIChE J.*, **12**, 522 (1966).
29. Millikan, C. B., "Proc. 5th Intern. Congr. Appl. Mech.", p. 386, John Wiley, New York (1939).
30. Oliver, D. R., *Can. J. Chem. Eng.*, **44**, 100 (1966).
31. Patterson, G. K., and Zakin, J. L., *AIChE J.*, **13**, 513 (1967).
32. Phillips, O. M., *J. Fluid Mech.*, **27**, 131 (1967).
33. Rotta, J., *Ing. Arch.*, **24**, 258 (1956).
34. Sandborn, V. A., *Natl. Advisory Comm. Aeron. TN 3266* (1955).
35. Savins, J. G., *Soc. Petrol. Eng. J.*, **4**, 203 (1964); *Rheol. Acta*. **6**, 323 (1967).
36. ———, *AIChE J.*, **11**, 673 (1965).
37. Schlichting, H., "Boundary Layer Theory," 4th Ed., McGraw-Hill, New York (1960).
38. Seyer, F. A., Ph.D. thesis, Univ. Delaware, Newark (1968).
39. Seyer, F. A., and A. B. Metzner, *Can. J. Chem. Eng.*, **45**, 121 (1967).
40. Shertzer, C. R., Ph.D. thesis, Univ. Delaware, Newark (1965).
41. Singh, K., Ph.D. thesis, Pennsylvania State Univ., University Park (1966).
42. Tomita, Y., *Bulletin Jap. Soc. Mech. Eng.*, **9**, 730 (1966).
43. Townsend, A. A., "The Structure of Turbulent Shear Flow," Cambridge Univ. Press, Cambridge (1966).
44. Virk, P. S., et al. *J. Fluid Mech.*, **30**, 305 (1967).
45. Wells, C. S., J. Harkness and W. A. Meyer, LTV Research Center Rept. No. 0-71000/6R-22, submitted for publication, (1966).
46. Wells, C. S., Jr., Am. Inst. Aeron. Astronaut, J. **3**, 1801 (1965).
47. ———, and J. G. Spangler, *Phys. Fluids*, **10**, 1890 (1967).
48. White, J. L., and A. B. Metzner, *J. Appl. Polymer Sci.*, **7**, 1863 (1963).

Manuscript received Dec. 4, 1967. Revision received March 28, 1968; paper accepted April 14, 1968.

Mutually Dependent Heat and Mass Transfer in Laminar Duct Flow

E. M. SPARROW
University of Minnesota, Minneapolis, Minnesota

and T. S. CHEN
University of Missouri, Rolla, Missouri

An analysis is performed of the strongly coupled heat and mass transfer processes which result from sublimation of mass from the walls of a duct into a flowing gas, the latent heat being provided solely by convective transfer from the gas. The flow is assumed to be laminar and hydrodynamically developed. Results are given for the streamward variations of the bulk and wall temperatures and mass fractions, of the heat and mass transfer rates, and of the local heat transfer coefficient. Representative temperature and mass fraction profiles are also presented. Entrance lengths characterizing the near approach to fully developed conditions are tabulated. Comparisons are made of the present results (based on a parabolic velocity profile) with those based on a slug flow velocity profile. A subsidiary analysis using the Lévêque model is also performed and the results compared with those of the principal solution.

Heat transfer processes in duct and tube flows have been the subject of extensive analytical investigation for many years (*1*). In recent years, mass transfer processes in internal flows have also been studied analytically [for